ISSN NO. 2320–7418 DOI: 10.22270/jmpas.V10I5.1454

International peer reviewed open access journal

Journal of Medical Pharmaceutical and Allied Sciences

Journal homepage: www.jmpas.com CODEN: JMPACO

Case report

Lung nodule semantic segmentation with bi-direction features using U-INET

Eali Stephen Neal Joshua[1*], Debnath Bhattacharyya[2], Midhun Chakkravarthy[2]

1. Lincoln University College, Kuala lumpur, Malaysia
2. Koneru Laksmaiah Education Foundation, Greenfield, Vaddeswaram, Guntur, India

ABSTRACT

It's difficult to detect lung cancer and determine the severity of the disease without a CT scan of the lungs. The anonymity of nodules, as well as physical characteristics such as curvature and surrounding tissue, suggest that CT lung nodule segmentation has limitations. According to the study, a new, resource-efficient deep learning architecture dubbed U-INET is required. When a doctor orders a computed tomography (CT) scan for cancer diagnosis, precise and efficient lung nodule segmentation is required. Due to the nodules' hidden form, poor visual quality, and context, lung nodule segmentation is a challenging job. The U-INET model architecture is given in this article as a resource-efficient deep learning approach for dealing with the problem. To improve segmentation operations, it also includes the Mish non-linearity functions and mask class weights. Furthermore, the LUNA-16 dataset, which included 1200 lung nodules, was heavily utilized to train and evaluate the proposed model. The U-INET architecture outperforms the current U-INET model by 81.89 times and reaches human expert level accuracy.

Keywords: Lung Cancer, ReLU, U-NET, BiFN, Lung node Segmentation, Convolutional Neural Network

Received - 30-06-2021, Reviewed - 24/07/2021, Revised/ Accepted- 07/09/2021

Correspondence: Eali Stephen Neal Joshua* ✉ stephen_neal@lincoln.edu.my

Lincoln University College, Kuala Lumpur, Malaysia

INTRODUCTION

The World Health Organization (WHO) projected that there would be about 10.4 million people [1] with lung cancer and more than 1.6 million deaths as a result of lung cancer in 2020 based on the most recent American Centres for Disease Control and Prevention data. A diagnosis of lung cancer may include one or more of the following conditions: pulmonary TB, pneumonia, effusion, tumour, or infiltration [2]. When individuals have an infection in their chest, it is referred to as a lung infection, and it has the potential to lead to cancer of the respiratory system in certain cases. It is essential that the identification and examination of these malignant nodules in the lungs be done as soon as feasible [3], else they may spread. Without doing so, the patient's mortality rate increases, and the treatment procedure takes longer, resulting in a slower treatment process. Computed tomography [4] scans are a very precise imaging technique intended for the identification and assessment [5] of lung nodules, but they have been widely abandoned due to their high cost. These CTs are a good example of scans is acquired using noise CT scanners, which utilise multiple detectors. This type of fine segmentation of the nodules in the lung are catastrophic [6], as it can have a dramatic impact on later results. On the other hand, to properly diagnose a patient, a radiologist must first perform a CT scan which features approximately 160-600 slices [7], which is a time-consuming and difficult task. Additional, separating amongst the lung, testicular [8], protrusions, and knobs is difficult, as the protrusions and knobs all have a similar appearance. For example, if a nodule appears to be attached to the lung wall or a vessel in the lung tissue, it is extremely difficult to determine where the nodule ends and the rest of the lung tissue begins. With regard to the lengthy and cumbersome process of manually segregating [9] lung nodules via a simple threshold and morphological-based method, it must be taken into consideration that there is significant variation in the size and type of nodules.

Figure 1. Showing the Benign and Malignant Nodules on LUNA 16

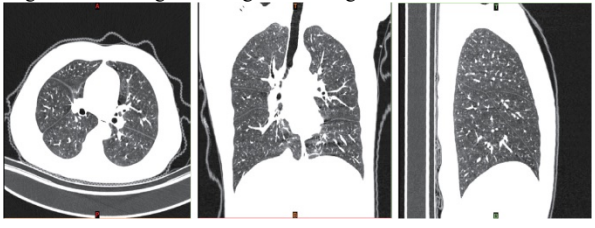

To distinguish between the two types of nodules, adhesion-type nodules, such as juxta pleural, pleural, and juxta vascular nodules, as well as ground-glass opacity nodules, are distinguished; to distinguish between the two types of (water) chestnut nodules, Extra tests for segmentation of nodules with trivial thickness and intensity are also conducted in the segmentation of nodules with a negligible quantity of noise around them, in addition to the tests already performed. Selling at a loss was such a disincentive that it essentially prevented the network from expanding its capacity to offer more complex characteristics, and as a result, the network's ability to down sample a portion of its data has been severely restricted as a result. The findings of this study have a significant impact on the accuracy of feature map abstraction for big nodules, which is a significant improvement over previous work. Consequently, a segmentation network is needed to accommodate the different kinds of nodules that are targeted by this system [10] for the reasons stated above (including small, medium, and large nodules).

BACKGROUND AND RELATED WORKS

[11], Accurate and effective segmentation of CT scans is needed to help treat lung cancer. They propose a dilated convolution-based U-INET network (DC-U-NET) and compare segmented lung CT results with DC-U-NET, Otsu, and region growth. The IOU Intersection, Dice coefficient, Precision, and Recall are used to evaluate the algorithms. The segmented image of DC-U-INET is closer to the ground truth than Otsu and region growing. DC-U-INET has an IOU of 0.9627. This model improves the previous segmentation process while shortening the time it takes to segment lung, blood vessels, trachea, and other organs.

[12] To determine whether larger nodules had a higher cancer-initiating rate, U-INET was used to segment nodules smaller than 15 mm with a segmentation that uses 2D. On-screen backgrounds are typically disregarded in favour of foreground labelling. The nodule is smaller than the rest of the image. We used the dice coefficient loss function in this study. U-proposed Net's pre-processing method utilizes complementary labelling as input. Labelling is exchanged here. the position is not nodding, the label goes away. The findings of this study hold up to minimal data. In a small number scenario, complementary labelling may be used. Data pre-processing can make the results for finding lung nodules considerably better.

[13], This study has found an automated method for segmenting skeletal muscle area at L3. This tool is an efficient way to assess skeletal muscle area in cancer patients, which may have some applications on low-quality CT scans of patients with cancer.

[14], Seg-Unet: combining global and patched approaches to handle bone lesions of all shapes, sizes, and rareness. Our model is integrated and includes various segments of the tumour as well as specialized modules for each. Patch-based modelling helps us find tumours faster. Chonnam National University Hospital's doctors funded the Lung Tumor dataset (CNUH). The experiment shows that our method outperforms the competition with a 99.05% accuracy and an average Mean IoU of 84.84%. Our findings showed a notable impact on lung tumour detection.

[15] Retroactive to include 915 patients with solitary solid pulmonary nodule characteristics and CT findings were found. A U-NET-based DL model was used for tumour segmentation and radiomics feature extraction in 3D. We found that intramodular, peri-nodular, and gross nodular radiomics features are the maximum relevance and minimum redundancy. A preoperative DL (IDL) was proposed to differentiate healthy tissues from gated nodes. five-fold cross-validation was used to select and rate the models were assessed using ROC and calibration curves. The CIRDL outperformed the IDL, CIDL, intra-RDL, peri-RDL, and gross-RDL models, all of which had AUCs below 0.8322. A new diagnostic tool, CIRDL, that distinguishes between granuloma nodules and solid lung cancer nodules is in the works.

[16] ResNet-34 network (referred to as Res BCDU-NET). We use the BConvLSTM (Bidirectional Convolutional Long Short-term Memory) as an advanced integrator module. This wants to merge the feature maps obtained when the previous up-convolutional layer was expanded. Convolutional dense layer finally applied for path contraction. This confirmed the method's effectiveness, where a dice coefficient index of 97.31% was obtained.

[17] (3D U-INET separate lung model) (3D U-INET separate lung model). (2D U-INET whole lung model, Dice similarity coefficients were 98.4 ± 1.0 percent) (2D U-INET separate lung model). (Dice similarity coefficients were 97.9 ± 1.3 percent 2D U-INET whole lung model and 98.0 ± 1.2 percent (2D U-INET lung model)) (2D U-INET separate lung model).

[18], It relies on Deep Learning and SegNet for the same goal. We are investigating the most promising tools for nodule characterization. LIDC nodules were used, achieving Dice scores of 0.663, 0.830, and 0.823 for the SBF, U-NET, and SegU-NET. Therefore, U-NET-based models yield more comparable results, making them more reliable for the proposed exercise. It had similar results to the U-NET, but was easier to use and more memory efficient. Additional research may aid the implementation of this model in a decision support system and assist physicians in diagnosing lung pathology.

[19] Using the 2D U-NET, which does not require high-performance computational resources, the lungs were separated into two lobes. Lung cancers with significant radiation treatment can benefit from semantic segmentation and deep learning.

[20] In a 2D pipeline, using the strengths of U-INET for pixel-wise segmentation, and Mask R-CNN, for instance, detection, we combine a loss function that incorporates data imbalance, which occurs when an image has an imbalanced ratio of dark to light pixels, and Mask-R-CNN, which performs case recognition, to form a pipeline that features improved pixel-wise segmentation within bounding boxes. A final stage, which is comprised of a label refinement algorithm and 3D instance detection with a tracking approach along the slicing dimension, applies a pixel-wise labelling modification and 3D case recognition. In this example, instances have been detected and represented by a 3D pixel-wise mask, bounding volume, and centroid position.

[21] To process and validate a completely computerized lung lobe segmentation technique, a 3D U-INET was used. A total of 196 chest CT scans were obtained from healthy and mildly-to-moderately ill patients. Individually, the examination remained segmented using a traditional image dispensation method, and gold standards were created manually by a radiologist. The part regions in the CT images were segmented using a U-INET architecture and a deep CNN on separate training, validation, and test datasets. The authors from [16-26] have proposed their work with the same potential of data, as a result the robustness of the model was missing. If the U-INET was applied to the different variety of data, U-INET was ultimately missing the IOU intersection and dice co-efficient index accuracy. However, the proposed model U-INET was applied on the variety of data and shows impressive results when compared with other benchmark models. We have tested our model on the diversity of data in LUNA 16 benchmark dataset.

RESOURCES AND APPROACHES

Proposed Model Architecture

U-INET Architecture

Additional layers of pooling, including max pooling, ReLU activation, concatenation, and up sampling, are part of the U-INET model [22]. This passage is about the various ways in which the business is being affected by the slow economy. The section in front of you contains four distinct contraction blocks. Before performing a 2*2 max pooling, every contraction block takes in an input and applies two 3*3 ReLu convolution layers before producing an output. As the pooling layers are stacked, the number of feature maps increases by a factor of two. The layer immediately preceding the bottleneck [23] is composed of two 3*3 convolution layers and two 2*2 convolution layers. A vast expanse of circuitry, each block providing input to multiple convolutional layers before sending their combined signals on to two 3*3 convolutional layers and a 2*2 sampling layer, constitutes the entirety of the expansion section. In addition, the pipeline concatenates the feature map for the contracting path with the feature map for the expanded path.

As the last step, a 1*1 Conv layer is used to equalize [24] the number of feature maps and segments, thereby adjusting the number of dimensions in the output. We use a loss function to compute a loss value for each pixel in the image in U-NET. Combining this with the previous feature will enable the identification of cells within the segmentation map for increased efficiency. Before a pixel can be put into the SoftMax function, it first goes through the SoftMax function. This process is known as the loss function. Figure 1 shows the basic block diagram of U-INET Architecture. Segmentation [25], which used to be an organization problem, has been transformed into a classification problem, in which each pixel must be classified into one of the classes.

Figure 2. Showing Basic Architecture of U-INET Architecture [31]

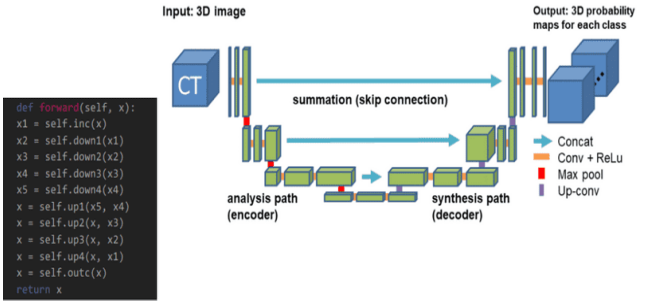

UNET for Bidirectional Features Network

In the realm of medical imaging segmentation, deep learning approaches are showing capable outcomes. UNET, one of the most well-known architectural designs in the world, could be used as a Nodule Candidate Point Generation target for us. Annotated datasets are used to train these networks in this setting. No training data is required for the methods for generating candidate points utilized in the image processing. When we train our UNET model, we use the LUNA16 dataset. The presence of nodule sites and their radius, as well as the CT scan value used to generate the binary mask for each scan in the dataset, are all included in LUNA16. For the first topic, I would want to discuss the LUNA16 dataset's pre-processing [26]. CT scans are saved in. mmh files, and SimpleITK is used to import the scan image into memory. We have defined three functions for me: Each CT image in the LUNA16 dataset is labelled with nodule spots and the radius of the nodule, which are used in the binary mask generation procedure. To get things started, let us speak about how the LUNA16 dataset was pre-processed. Simple ITK is used to read the CT scans, which are saved in '. MHD' files. The following are the functions that I have defined:

- Load_ itk - Used to read a CT scan for the '. MHD' file.
- World_ 2_voxel- Convert world coordinates to voxel coordinates.
- Voxel_2_world- Convert voxel coordinates to world coordinates.

DATA AND EXPERIMENTS

Dataset

For the experiments testing of the U-INET proposed model, the approach we utilized is Benchmark dataset available on LUNA 16 (Lung Nodule Analysis 2016) [27] grand Challenge. LUNA 16 is resulting from the "Lung Image Database Consortiums Images Collection (LIDC/IDRI)". Input folder have main three things; one is for the sample CT scan images with sample_1_images. The stage_labels folder contains the ground truth of the satge1 training set of images, and stage_submission shows the format of the submission for stage_1.

Table 3. Showing the Various distribution features of LUNA 16 Dataset and was shown in the standard deviation format

Characteristics	Training Set	Testing Set
Malignancy	2.96±0.96	3.04±1.02
Spiculation	1.61±0.80	1.66±0.88
Subtlety	3.92±0.84	4.08±0.79
Lobulation	1.74±0.74	1.83±0.81
Diameter in mm	8.14±4.59	9.08±5.25
Margin	4.04±0.84	4.07±0.78

Table 3 shows the various feature extraction values from the LUNA 16 database. Malignancy shows the range of presence of characteristics within the node. Spiculation specifies the coordinate's outline of the node. Subtlety is the region around the nodule. Lobulation is the shape and its characteristics of the nodule. Length of the nodule is calculated by the diameter and it's in mm. Margin indicates the area of the nodule region that's clarity. Histograms of the LUNA 16 dataset were shown in Figure 7 below.

Figure 3: Showing Histogram of the Luna 16 Dataset and Nodule sizes

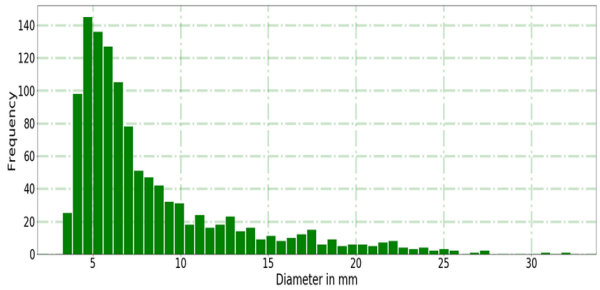

The benchmark dataset, that is, Database Resource Initiative containing a CT scan with a slice thickness of 2.6 mm were not included in the dataset. A total of 888 images were considered for the experimentation purpose. The images of LIDC/IDRI were annotated by four experienced radiologists and a two-phase annotation process was used for the process and it's a benchmark. The nodules of size above 3mm were considered by all four radiologists. 1186 annotations were present in the annotations file in the LUNA 16 dataset and a property file that is enhanced which indicates the properties of the nodules. After Post dispensation, [28] a total of 1167 CT scan metaphors consistent truth minced masks were portioned into two separate testing and training sets separately as 244 and 922 correspondingly. As represented in table 1, the two sets indistinguishable statistics distributions and their features.

Approximation performance

Dice similarity index co-efficient (F1) score is the main limitation performance matrix for the evaluation of the proposed U-INET segmentation model. To calculate the outcome of the two segmentation, the most common performance metrics were Dice similarity coefficient (DSC-F1). And, positive predictive value PPv and sensitivity was used as supplementary assessment parameters. The assessment performance system of measurement is articulated below:

$$DC = \frac{2 * V(Pq \cap Qr)}{V(pq) + V(QR}$$

$$Sens = \frac{V(Pq \cap Qr}{V(Pq)}$$

$$PP = \frac{V(Pq \cap Qr)}{V(Qr)}$$

Here "Pq" is used to represent "ground truth label", "Qr" is for the results of segmentation of images and 'V' is used for the voxels units measured in terms of volume size.

Implementation details

To carry out the experiment, Mish activation was utilized for efficient model training, and data augmentation was done on the LUNA 16 benchmark dataset to improve the proposed model's performance and resilience. To avoid overfitting using the model, we implemented a new technique that involves ending strategy training early if the model's performance does not increase. Model training will be stopped after every 20 epochs. Adam's Optimizer was utilized to get the most out of the system. All of this research was done with the Pytorch 1.8 stable version of the Deep Learning Framework GPU version, Python 3.8 programming language for development, and a CUDA capable NVIDIA GPU for increased training and performance. Experiments were conducted on a Microsoft Azure infrastructure with four CPUs and a 1TB SSD, and the training process took about nine hours to complete.

We mention techniques in the kernel which will aid in a deeper understanding of the problem statement and data visualization. Matplotlib, NumPy, skimage, and pydicom are the libraries that will be used to interpret, process, and visualize data in the model. The images are (z, 512, 512) pixels in size, with z representing the number of slices in the CT scan that varies depending on the scanner's resolution. The segmented lungs can also be used to identify lung nodule candidates and regions of relevance that could aid in better CT scan classification. Since there are nodules attached to blood vessels or present at the lung region's border, locating the lung nodule regions is a difficult task. Cutting 3D voxels around lung nodule candidates and moving them through a 3D CNN trained on the LUNA16 dataset can be used to further classify them. The

position of the nodules in each CT scan is included in the LUNA 16 dataset, which can be used to train the classifier.

RESULTS AND DISCUSSION

Abscission Study

The Abscission study experiment was based on the U-INET semantic segmentation architecture has been planned. Abscission experiment checks weather each and every component of the U-INET architecture for the effectiveness and performance of the proposed algorithm. The experiment results of the Abscission study were clearly tabulated in Table 4.

Outcome of Mish Activation Function

Mish activation functions were compared with the ReLU activation functions of the original U-INET architecture, instead of the ReLU activation functions of the U-INET architecture. U-INET indicates the Mish activation function in conjunction with other U-INET Mish indications. Therefore, we have to consider the likelihood that the mish model activation is lagging in the U-INET experiment.

Result of ReLU Activation Function

ReLU activation functions were implemented with the proposed U-INET segmentation architecture, which performed slightly lesser to the Mish Activation. Thus, with addition of the ReLU activation function to the U-INET architecture, a dice co-efficient of 81.89 % was achieved. When we compared the ReLU with Mish activation functions, a difference of 4.38 % variation can be observed. Thus, it can be observed that Mish outperformed ReLU activation function.

Result of BiFPN with ReLU activation function

From table 3, by replacing the basic backbone of the U-INET semantic segmentation with the Bi-directional Feature Network with ReLU activation function, the situation can be experimental that the architecture shows a good development of 79.22%.

Inference of the Abscission study

In Table 3, with reflection of the Dice coefficient index (F1) of U-INET Model (81.83%), it is clearly manifest that the proposed U-INET has shown the noteworthy development over U-INET+ ReLU, U-INET+ReLU+BIFPN and U-NET+ Mish Activation. As shown in Figure 8, the ‘histogram’ of the Dice coefficient value index values.

Figure 4. Showing Dice CO-efficient on LUNA 16 Dataset

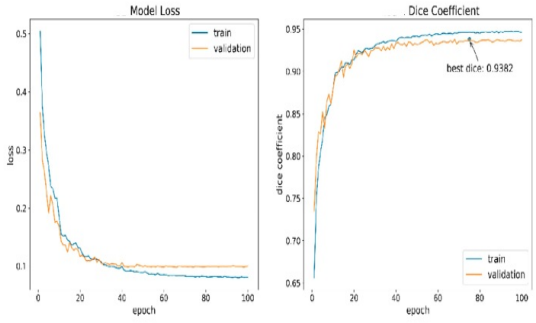

Table 4. Showing the Abscission study on LUNA 16 Testing test set and done on U-INET model.

Method	Dice-Co-efficient (%)	Sensitivity (%)	Positive Predictive Value (%)
U-NET	77.84±21.79	78.98±25.53	83.54±22.55
U-NET+BFPN	81.22±23.02	79.89±25.85	84.89±22.89
U-NET+ReLU	78.84±12.52	84.45±13.56	77.32±14.45
U-NET+ReLU+BFPN	79.22±12.36	91.69±13.78	77.94±14.35
U-INET	81.89±11.71	90.24±13.15	77.92±17.89

Total performance

As shown in Figure 8, the ‘histogram’ of the Dice coefficient value index values and the whole quantity of nodes, each of which was counted and centred on every trial in the test set, were designed for easier assessment of the production of the U-INET model on the test set.

Figure 5. Showing the visual segmentation of the Proposed Algorithm on various Heterogeneities of Lung Nodules

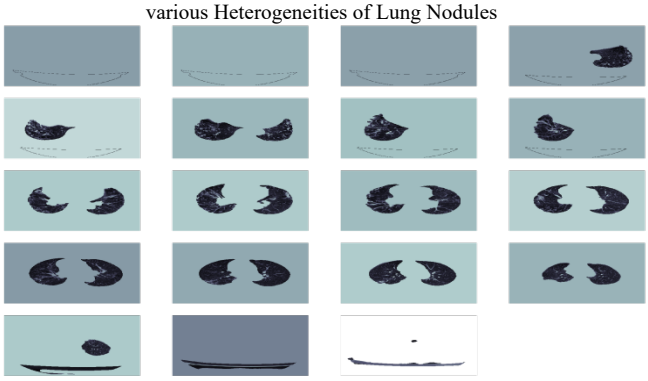

Figure 6. Showing FROC curve on the LUNA 16 Dataset

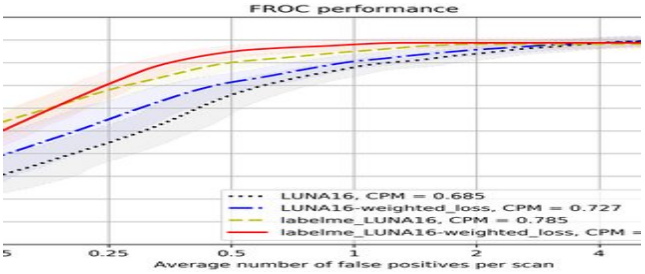

CONCLUSION AND FUTURE WORK

A simpler U-INET design for lung nodule segmentation is described in this paper. The design includes a network that utilizes a weight distribution and a bidirectional feature to effectively identify lung nodules. The feature enricher, Mish, Multi-Scale Feature Fusion, combines multi-scale feature fusion to serve as a feature extraction, and the model utilizes the support U-INET architecture to extract and decode feature maps. A Luna dataset is LUNA16. After an inspection and image processing of the proposed method's findings, the dice similarity coefficient for the LUNA16 dataset was determined to have a promising accuracy in the segmentation of lung nodes, with an 82.83 percent likeness constant. Lacunar, microscopic, and juxta pleural nodules, which have smaller or more complicated features, may be consistently distinguished with reasonable ease in situations

when the U-INET model cannot successfully segment them. In cooperation with U-INET, future study will concentrate on creating 3D Capsule Network that contains all essential components for fully automated lung cancer malignancy categorization.

CONFLICT OF INTEREST

No potential conflict of interest relevant to this article exists.

ACKNOWLEDGMENT

To Debnath Bhattacharyya for his continuous support in the results and study of this research.

REFERENCES

1. Long, F, 2020. Microscopy cell nuclei segmentation with enhanced U-NET. BMC Bioinformatics 21, 8.
2. Ayalew, YA, Fante, KA, Mohammed, M, 2021. Modified U-INETfor liver cancer segmentation from computed tomography images with a new class balancing method, BMC biomed eng 3, 4.
3. Rajagopalan, K, Babu, S, 2020. The detection of lung cancer using massive artificial neural network based on soft tissue technique, BMC Med Inform Decis Mak 20, 282.
4. Joshua, ESN, Chakkravarthy, M, Bhattacharyya, D, 2020. An extensive review on lung cancer detection using machine learning techniques: A systematic study, Revue d'Intelligence Artificielle, Vol 34, No 3, pp 351-359.
5. Kamel K, Mohammed, Aboul Ella Hassanien, Heba M Afify, 2021. 3D image segmentation for lung cancer using V Net architecture based deep convolutional networks, Journal of Medical Engineering & Technology, 45:5, 337-343.
6. Baek, S, He, Y, Allen, BG, 2019. Deep segmentation networks predict survival of non-small cell lung cancer, Sci Rep 9, 17286.
7. Sori, WJ, Feng, J, Godana, AW, 2021. DFD-Net: lung cancer detection from denoised CT scan image using deep learning. Front, Comput, Sci 15, 152701.
8. Saood, A, Hatem, 2021. I COVID-19 lung CT image segmentation using deep learning methods: U-INETversus SegNet, BMC Med Imaging 21, 19.
9. Kuan-bing Chen, Ying Xuan, Ai-jun Lin, Shao-hua Guo, 2021. Lung computed tomography image segmentation based on U-INET network fused with dilated convolution, Computer Methods and Programs in Biomedicine, Volume 207.
10. Chiu, TW, Tsai, YL & Su, SF, 2021. Automatic detect lung node with deep learning in segmentation and imbalance data labeling, Sci Rep 11, 11174.
11. Amarasinghe Kaushalya C, Lopes Jamie, Beraldo Julian, Kiss Nicole, Bucknell Nicholas, Everitt Sarah, Jackson Price, Litchfield Cassandra, Denehy Linda, Blyth Benjamin J, Siva Shankar, MacManus Michael, Ball David, Li Jason, Hardcastle Nicholas, 2021. A Deep Learning Model to Automate Skeletal Muscle Area Measurement on Computed Tomography Images, Frontiers in Oncology, volume 11.
12. Xiaofeng Lin, Han Jiao, Zhiyong Pang, Huai Chen, Weijie Wu, Xiaoyi Wang, Lang Xiong, Biyun Chen, Yihua Huang, Sheng Li, Li Li, 2021. Lung Cancer and Granuloma Identification Using a Deep Learning Model to Extract 3-Dimensional Radiomics Features in CT Imaging, Clinical Lung Cancer, ISSN 1525-7304.
13. Jalali, Y, Fateh, M, Rezvani, M, Abolghasemi, V, Anisi, M H, 2021. Res BCDU-NET: A Deep Learning Framework for Lung CT Image Segmentation, Sensors, 21(1), 268, MDPI AG.
14. Rocha, J, Cunha, A, Mendonça, AM, 2020. Conventional Filtering Versus U-INETBased Models for Pulmonary Nodule Segmentation in CT Images, J Med Syst 44, 81.
15. Takafumi Nemoto, Natsumi Futakami, Masamichi Yagi, Atsuhiro Kumabe, Atsuya Takeda, Etsuo Kunieda, Naoyuki Shigematsu, 2020. Efficacy evaluation of 2D, 3D U-INETsemantic segmentation and atlas-based segmentation of normal lungs excluding the trachea and main bronchi, Journal of Radiation Research, Volume 61, Issue Pages 257–264,
16. Bouget, D, Jørgensen, A, Kiss G, 2019. Semantic segmentation and detection of mediastinal lymph nodes and anatomical structures in CT data for lung cancer staging, Int J CARS 14, 977–986.
17. Bhattacharyya, D, Kumari, N M J, Joshua, E S N, & Rao, N T, 2020. Advanced Empirical Studies on Group Governance of the Novel Corona Virus, MERS, SARS and EBOLA: A Systematic Study, Int J Cur Res Rev| Vol, 12(18), 35.
18. Kumari, N M J, & Krishna, K K, 2018. Prognosis of Diseases Using Machine Learning Algorithms: A Survey, In 2018 International Conference on Current Trends towards Converging Technologies (ICCTCT) (pp. 1-9), IEEE.
19. Md Fashiar Rahman, Tzu-Liang (Bill) Tseng, Michael Pokojovy, Wei Qian, Basavarajaiah Totada, Honglun Xu, 2021. "An automatic approach to lung region segmentation in chest x-ray images using adapted U-INETarchitecture", Proc SPIE 11595, Medical Imaging Physics of Medical Imaging, 115953I.
20. Joshua, ESN, Chakkravarthy, M, Bhattacharyya, D, 2020. An extensive review on lung cancer detection using machine learning techniques: A systematic study, Revue d'Intelligence Artificielle, Vol 34, No 3, pp 351-359.
21. Aryan Ghazipour, Benjamin Veasey, Albert Seow, Amir Amini, 2021. "3D U-INETfor registration of lung nodules in longitudinal CT scans", Proc, SPIE 11597, Medical Imaging 2021: Computer-Aided Diagnosis, 115972S.
22. Lin L, Wu J, Cheng P, Wang K, Tang X, 2021. BLU-GAN: Bi-directional ConvLSTM U-INETwith Generative Adversarial Training for Retinal Vessel Segmentation, Intelligent Computing and Block Chain, FICC 2020. Communications in Computer and Information Science, vol 1385, Springer, Singapore.
23. Eali Stephen Neal Joshua, Debnath Bhattacharyya, Midhun Chakravarthy, Yung-Cheol Byun, 2021. "3D CNN with Visual Insights for Early Detection of Lung Cancer Using Gradient-Weighted Class Activation", Journal of Healthcare Engineering, vol 2021, Article ID 6695518, 11 pages.
24. Cui, L, Li, H, Hui, W, 2020. A deep learning-based framework for lung cancer survival analysis with biomarker interpretation, BMC Bio informatics 21, 112.

How to cite this article

Eali Stephen Neal Joshua, Debnath Bhattacharyya, Midhun Chakkravarthy, 2021. “Lung nodule semantic segmentation with bi-direction features using U-INET”. Jour. of Med. P’ceutical & Allied. Sci. V 10 - I 5, 1454, P- 3494-3399. doi: 10.22270/ jmpas.V10I5.1454